Microtubular Self-Assembly of Covalent Organic Frameworks

Bappaditya Gole, Vladimir Stepanenko, Sabrina Rager, Matthias Grüne, Dana D. Medina, Thomas Bein, Frank Würthner, and Florian Beuerle*

Dedicated to Sir Fraser Stoddart on the occasion of his 75th birthday

Abstract: *Despite significant progress in the synthesis of covalent organic frameworks (COFs), reports on the precise construction of template-free nano- and microstructures of such materials have been rare. In the quest for dye-containing porous materials, a novel conjugated framework **DPP-TAPP-COF** with an enhanced absorption capability up to λ = 800 nm has been synthesized by utilizing reversible imine condensations between 5,10,15,20-tetrakis(4-aminophenyl)porphyrin (**TAPP**) and a diketopyrrolopyrrole (**DPP**) dialdehyde derivative. Surprisingly, the obtained COF exhibited spontaneous aggregation into hollow microtubular assemblies with outer and inner tube diameters of around 300 and 90 nm, respectively. A detailed mechanistic investigation revealed the time-dependent transformation of initial sheet-like agglomerates into the tubular microstructures.*

The formation of well-defined nanoscale superstructures has been a major achievement for supramolecular chemistry in recent years.[1] To achieve precise control over function and materials properties, however, molecular organization must often be mastered over even larger spatial regimes, for example, on the μm scale.[2] In natural systems, function often emerges from defined microarchitectures that are assembled via protein-templated biomineralization.[3] While the defined bottom-up fabrication of artificial microstructures is still quite challenging, it would significantly improve the understanding of structure–property relationships for real applications.

Covalent organic frameworks (COFs), a class of crystalline porous polymers,[4] have recently emerged as promising materials for potential applications in gas adsorption,[5] energy storage,[6] heterogeneous catalysis,[7] and sensing.[8] In particular, two-dimensional (2D) COFs comprising extended π-systems or well-defined donor–acceptor heterojunctions in nm-sized regimes are promising candidates for optoelectronic applications.[9] In most cases, however, 2D COFs are prepared and isolated as microcrystalline powders. The limited long-range crystal growth and morphological definition is presumably due to internal defects[10] and kinetic trapping of smaller crystallites as a result of the dispersive π-stacking of individual layers. Defined morphologies such as belts,[11] fibers,[12] and spheres[13] have been observed for some COFs, but detailed mechanistic investigations have been conducted so far for only two examples of COF-based hollow spheres.[14] The template-assisted synthesis of COF nanotubes has also been reported.[15] However, in this case additional effort was required to initially prepare and finally remove the templates

[*] Dr. B. Gole, Dr. M. Grüne, Prof. Dr. F. Würthner, Dr. F. Beuerle
Universität Würzburg, Institut für Organische Chemie
Am Hubland, 97074 Würzburg (Germany)
E-mail: florian.beuerle@uni-wuerzburg.de

Dr. B. Gole, Dr. V. Stepanenko, Prof. Dr. F. Würthner, Dr. F. Beuerle
Center for Nanosystems Chemistry
& Bavarian Polymer Institute, BPI
Theodor-Boveri-Weg, 97074 Würzburg (Germany)

S. Rager, Dr. D. D. Medina, Prof. Dr. T. Bein
Ludwig-Maximilians-Universität München
Department of Chemistry & Center for NanoScience, CeNS
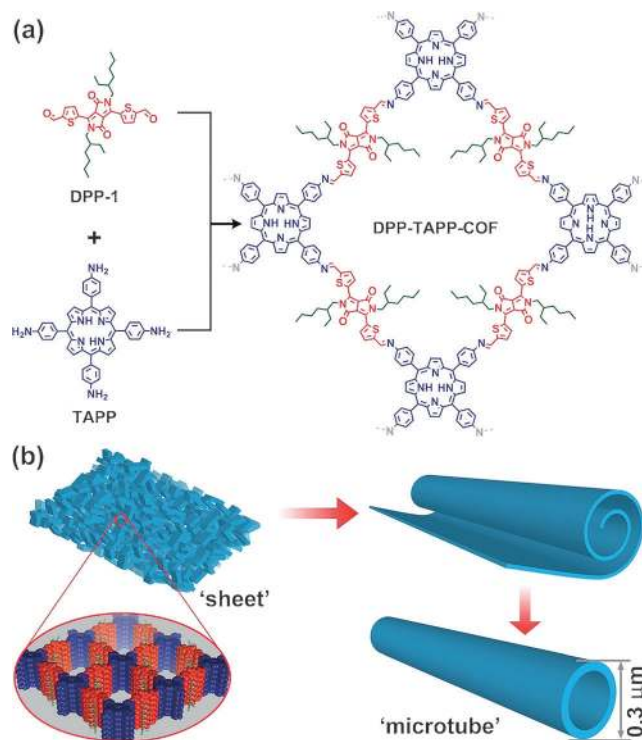Butenandtstrasse 5–13, 81377 München (Germany)

Figure 1. a) Synthesis and b) proposed self-assembly of **DPP-TAPP-COF** into microtubes.

without causing irreversible modifications of the COF properties.

Herein, we report on the synthesis of **DPP-TAPP-COF** which contains diketopyrrolopyrrole (DPP) and tetraphenyl-porphyrin (TPP) moieties. This imine COF adopts a unique hollow microtubular morphology with uniform diameters, rendering it, to the best of our knowledge, the first example for bottom-up microtubular self-assembly based on COF materials (Figure 1).

During our quest for dye-containing COFs, we studied the reaction of 5,10,15,20-tetrakis(4-aminophenyl)porphyrin (**TAPP**)[16] and the organic semiconductor DPP[17] dialdehyde derivative **DPP-1** bearing solubilizing ethylhexyl side chains. Microcrystalline precipitates were obtained after the AcOH-catalyzed solvothermal reaction of the two components in *n*-BuOH/mesitylene (3:1) at 120 °C for five days. The precipitates were washed with anhydrous THF and acetone and then dried under high vacuum to provide **DPP-TAPP-COF** (Figure 1a) as a dark purple material in 53 % yield. Remarkably, even small deviations from these optimized conditions resulted in only amorphous products (see Table S1).

Strikingly, scanning electron microscopy (SEM) and transmission electron microscopy (TEM) revealed that **DPP-TAPP-COF** predominantly assembles into well-defined microtubular structures (Figure 2) that extend up to 20 µm in
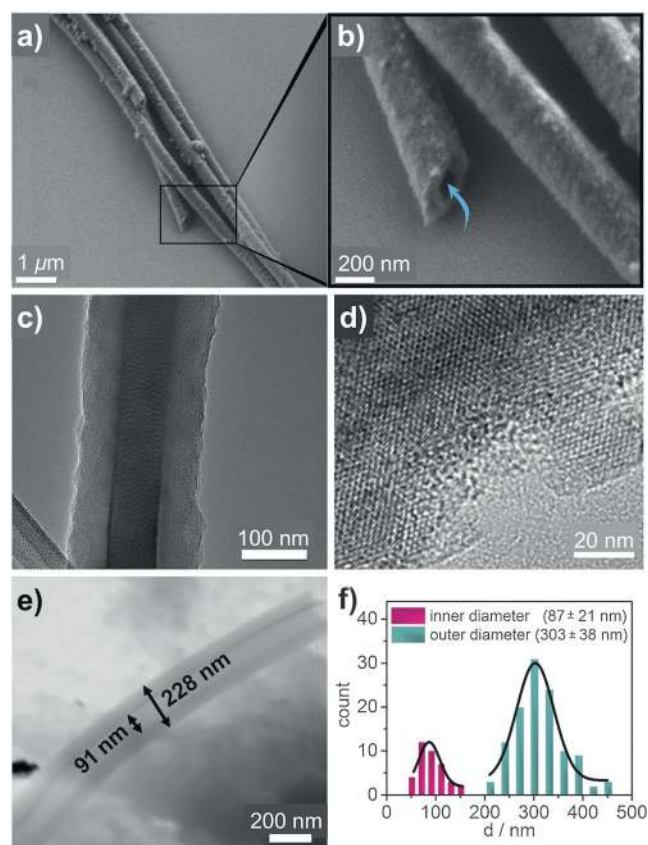
length. The majority of the microtubes were aggregated into bundles; in some cases, however, individual tubes were observed, which had possibly separated mechanically in the course of sonication during sample preparation. Energy-dispersive X-ray (EDX) spectroscopy on various positions of different tubes revealed a uniform atomic composition, thus indicating the homogeneous formation of a composite material (Figure S10). SEM and scanning transmission electron microscopy (STEM) images (Figures 2b,e) clearly demonstrated the hollow nature and remarkably smooth surface of the tubes. Statistical analysis yielded mean values for outer and inner diameters of $d = (303 \pm 38)$ nm and (87 ± 21) nm, respectively (Figure 2f), which corresponds to a mean wall thickness of $d = (105 \pm 9)$ nm (Figure S23). High-resolution TEM (Figure 2d) revealed a periodic rhomboidal framework with domain sizes in the range of several tens of nanometers.

Indeed, framework formation was proven by several analytical techniques. The FTIR spectrum (Figure S5) shows almost complete disappearance of the aldehyde band at $\tilde{\nu} = 1649$ cm^{-1} and the simultaneous generation of a new band at $\tilde{\nu} = 1582$ cm^{-1} corresponding to the C=N stretching mode. In addition, the N–H stretching band for the amino groups of **TAPP** at $\tilde{\nu} = 3316$ cm^{-1} is significantly weakened after polymerization. Similar spectral trends indicating identical functionalities and connectivity were observed for the model compound **M-1**, in which two **TPP** units are attached to one **DPP-1**. Solid-state ^{13}C cross-polarization magic-angle-spinning (CP-MAS) NMR spectra (Figure 3d–f) for both **DPP-TAPP-COF** and **M-1** are in excellent agreement with ^{13}C NMR solution data of **M-1** obtained in CDCl$_3$. The absence of any aldehyde signal, expected to appear beyond

Figure 2. a),b) SEM and c) TEM images of **DPP-TAPP-COF** nanotubes; d) high-resolution TEM image of a microtube's outer wall indicating crystalline domains; e) STEM image of single microtube indicating the hollow nature of the tube; f) statistical distribution of inner and outer tube diameters.
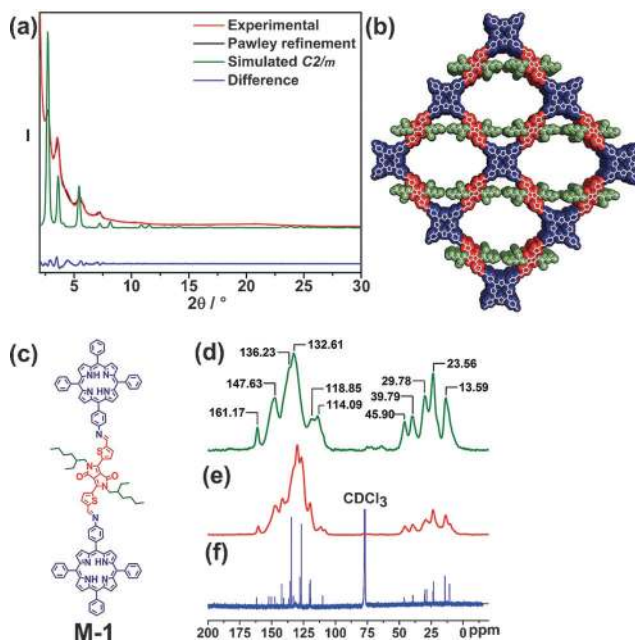

Figure 3. a) PXRD patterns of **DPP-TAPP-COF**: experimental (red), Pawley refinement (black), simulated pattern (green), and difference plot (blue). b) Simulated unit cell for a monoclinic crystal system of space group *C2/m*. c) Model compound **M-1**. d) Solid-state ^{13}C CP MAS NMR spectra of **DPP-TAPP-COF** and e) **M-1**. f) ^{13}C NMR spectrum (CDCl$_3$, 400 MHz, RT) of **M-1**.

$\delta = 180$ ppm, indicates virtually quantitative consumption of the DPP precursor. Elemental analysis of **DPP-TAPP-COF** supported the efficient formation of a polymeric material composed of both monomers (see the Supporting Information for details). Thermogravimetric analysis (TGA) revealed a thermal stability up to 350°C followed by a weight loss of around 20%, which is tentatively attributed to the loss of the alkyl side chains,[18] and ultimate decomposition at 450°C (Figure S6). Powder X-ray diffraction (PXRD) revealed Bragg reflections centered at low 2θ angles of 2.68°, 3.51°, 4.26°, 5.49°, and 7.17° corresponding to 110, 020, 120, 220, and 040 planes, respectively (Figure 3a), thus implying the formation of small COF domains. A simulated diffraction pattern in the monoclinic $C2/m$ space group (see the Supporting Information for details) with an eclipsed but slightly offset (≈ 1 Å) AA stacking provides a good description of **DPP-TAPP-COF** (Figure 3b). The final unit cell parameters were obtained by performing Pawley refinement and correspond to $a = 45.3$ Å, $b = 48.1$ Å, $c = 3.9$ Å; $\alpha = \gamma = 90°$, $\beta = 74.3°$ ($R_{wp} = 3.82\%$ and $R_p = 2.86\%$).

Nitrogen sorption analysis was performed after activation of the material at elevated temperatures under high vacuum for 12 hours. The obtained sorption isotherm (Figure S9) and calculated BET surface area of 139 $m^2 g^{-1}$ indicate a fairly low N_2 uptake, which we attributed to the offset stacking and primarily to the sterically demanding side chains protruding into the pores.
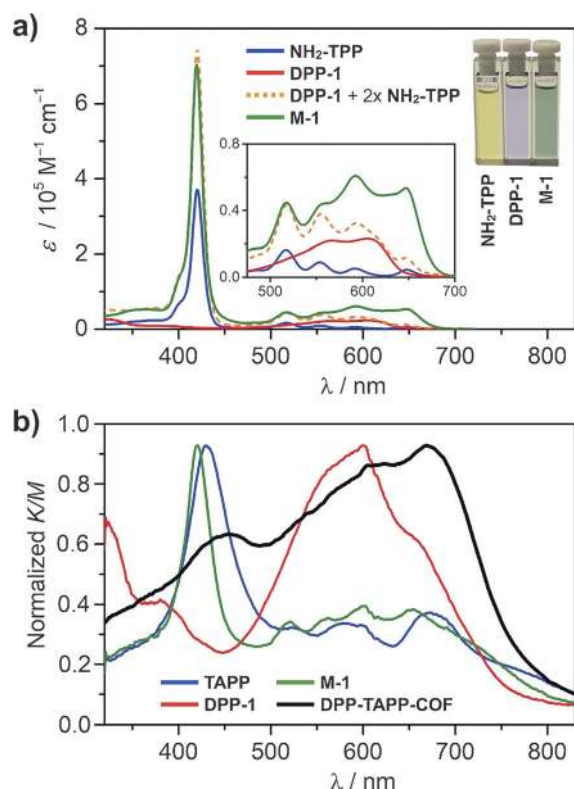

Figure 4. a) UV/Vis absorption spectra (CHCl₃, RT) of **M-1**, **NH₂-TPP**, and **DPP-1**. Insets show enlarged region from $\lambda = 500$ to 700 nm and the visual colors of the compounds in CHCl₃. b) Kubelka–Munk function for diffuse reflectance spectra of **DPP-TAPP-COF**, **M-1**, and precursors **TAPP** and **DPP-1**. Spectra are normalized to global absorption maximum.

The absorption spectrum of **M-1** nearly corresponds to an overlay of **NH₂-TPP** and **DPP-1**, except for slightly stronger Q-bands at $\lambda = 590$ and 650 nm (Figure 4a). Steric interactions of the phenyl rings with the porphyrin possibly induce a significant twist, thus resulting in limited π-conjugation. Diffuse reflectance spectra for **DPP-TAPP-COF** showed a significant shift of the maximum absorption to $\lambda = 670$ nm (Figure 4b), which can be rationalized by planarization of the π-system and pronounced aggregation of the individual layers within the COF.[16b] In addition, the ratio of the relative intensities of the Q-bands versus the Soret band increased from 0.4 and 0.41 for **TAPP** and **M-1**, respectively, to 1.47 for the COF. Due to this enhanced absorption, **DPP-TAPP-COF** more efficiently harvests photons in the visible and near-IR region.

For time-dependent morphological studies, COF reaction mixtures were distributed in several Pyrex tubes and quenched at different time intervals. SEM images after one day indicated the formation of plate-like agglomerates of small individual crystallites (Figure 5a). After four days, plates with significantly smoother surfaces were observed along with initial indications of the scrolling of some of the thin sheets (Figures 5b,c). After five days, hollow microtubes were isolated as the major product (Figure 5d) in addition to some remaining plate-like aggregates. A further increase of the reaction time up to 15 days resulted in roughening and fracturing of the tube walls as evidenced by SEM (Figures S17e,f) and PXRD (Figure S16). However, the isolated COF microtubes are stable for several months and PXRD measurements showed no indications of structural collapse. Based on these data, there is no evidence for tube growth via Ostwald ripening, as was recently invoked for the formation of spherical COF particles.[14a] Instead, we propose the following mechanism for microtube formation (Figure 5). Initially, small crystallites of imine condensation products are formed that agglomerate into sheet-like aggregates, which is presumably induced by van der Waals interactions between the branched alkyl chains. Over time, the initial crystallites grow further by condensation of unreacted precursors or grain boundary consumption via reactive aldehydes and amines at the interfaces (Figures S19 and S20). This transformation is supported by a change in thickness for the initial and uniform sheets from around 500 to 100 nm, respectively. Hence, we propose that the spontaneous scrolling into tubular arrangements (red arrows in Figure 5c) minimizes destabilizing interactions with solvent molecules, as was previously shown for supramolecular nanotubes[19] and microporous polymers.[20] This assumption is also supported by similar wall thicknesss for the microtubes and the uniform sheets. Subsequently, well-defined uniform nanotubes are generated presumably via dynamic imine formation of unreacted aldehyde and amino groups present at the edges.

In conclusion, we have demonstrated the successful implementation of DPP and TPP chromophores into one single conjugated COF via reversible imine condensations. UV/Vis studies revealed a significant red-shift after framework formation that was attributed to enhanced conjugation and delocalization along and across the COF sheets. Remarkably, **DPP-TAPP-COF** crystallites self-assemble into micro-
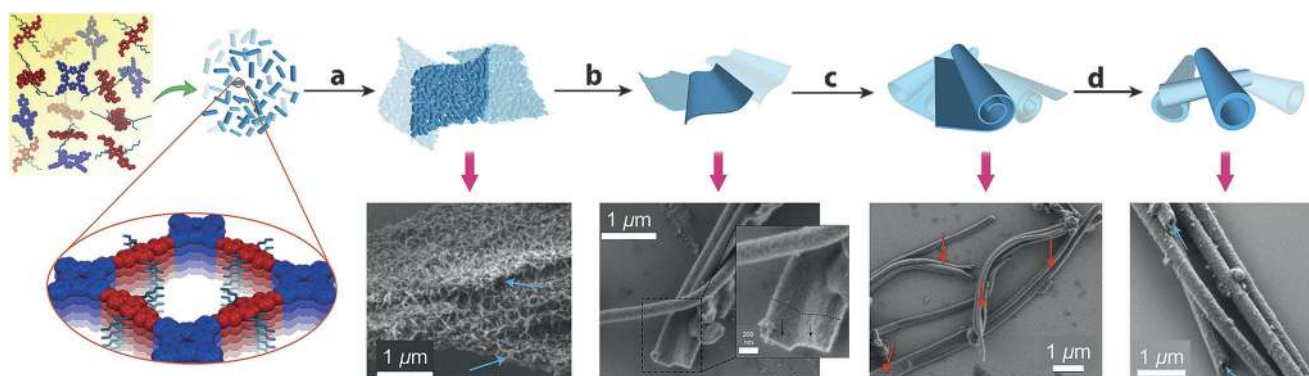
Figure 5. Proposed mechanism for microtube formation: a) agglomeration of small **DPP-TAPP-COF** crystallites into sheet-like aggregates, b) smoothing and densification of sheets by reversible imine condensations, c) rolling of the sheets, and d) tube formation and recombination by reversible imine condensations.

tubular aggregates with a narrow size distribution as evidenced by SEM and STEM images. Time-dependent studies support the hypothesis that the microtubes originate from rolled-up crystallite sheets. These findings pave the way for fascinating future experiments on single microtubes, as well as the inclusion of suitable guest molecules or even larger nanostructures, thus allowing additional fine-tuning of the materials properties.

Conflict of interest

The authors declare no conflict of interest.

[1] a) T. Aida, E. W. Meijer, S. I. Stupp, *Science* **2012**, *335*, 813–817; b) G. Zhang, O. Presly, F. White, I. M. Oppel, M. Mastalerz, *Angew. Chem. Int. Ed.* **2014**, *53*, 1516–1520; *Angew. Chem.* **2014**, *126*, 1542–1546; c) S. Klotzbach, F. Beuerle, *Angew. Chem. Int. Ed.* **2015**, *54*, 10356–10360; *Angew. Chem.* **2015**, *127*, 10497–10502; d) F. Würthner, C. R. Saha-Möller, B. Fimmel, S. Ogi, P. Leowanawat, D. Schmidt, *Chem. Rev.* **2016**, *116*, 962–1052.

[2] a) G. M. Whitesides, B. Grzybowski, *Science* **2002**, *295*, 2418–2421; b) J.-F. Lutz, J.-M. Lehn, E. W. Meijer, K. Matyjaszewski,

Nat. Rev. Mater. **2016**, *1*, 16024; c) X. Zhou, Q. Jin, L. Zhang, Z. Shen, L. Jiang, M. Liu, *Small* **2016**, *12*, 4743–4752.

[3] a) L. B. Gower, *Chem. Rev.* **2008**, *108*, 4551–4627; b) H. Cölfen, *Nat. Mater.* **2010**, *9*, 960–961.

[4] a) A. P. Côté, A. I. Benin, N. W. Ockwig, M. O'Keeffe, A. J. Matzger, O. M. Yaghi, *Science* **2005**, *310*, 1166–1170; b) E. L. Spitler, W. R. Dichtel, *Nat. Chem.* **2010**, *2*, 672–677; c) L. Ascherl, T. Sick, J. T. Margraf, S. H. Lapidus, M. Calik, C. Hettstedt, K. Karaghiosoff, M. Döblinger, T. Clark, K. W. Chapman, F. Auras, T. Bein, *Nat. Chem.* **2016**, *8*, 310–316; d) D. Rodríguez-San-Miguel, A. Abrishamkar, J. A. R. Navarro, R. Rodriguez-Trujillo, D. B. Amabilino, R. Mas-Ballesté, F. Zamora, J. Puigmartí-Luis, *Chem. Commun.* **2016**, *52*, 9212–9215; e) G. Lin, H. Ding, D. Yuan, B. Wang, C. Wang, *J. Am. Chem. Soc.* **2016**, *138*, 3302–3305; f) P. J. Waller, F. Gándara, O. M. Yaghi, *Acc. Chem. Res.* **2015**, *48*, 3053–3063; g) X. Feng, X. Ding, D. Jiang, *Chem. Soc. Rev.* **2012**, *41*, 6010–6022; h) N. Huang, P. Wang, D. Jiang, *Nat. Rev. Mater.* **2016**, *1*, 16068.

[5] a) S. S. Han, H. Furukawa, O. M. Yaghi, W. A. Goddard, *J. Am. Chem. Soc.* **2008**, *130*, 11580–11581; b) C. J. Doonan, D. J. Tranchemontagne, T. G. Glover, J. R. Hunt, O. M. Yaghi, *Nat. Chem.* **2010**, *2*, 235–238; c) Y. Zeng, R. Zou, Z. Luo, H. Zhang, X. Yao, X. Ma, R. Zou, Y. Zhao, *J. Am. Chem. Soc.* **2015**, *137*, 1020–1023.

[6] a) C. R. DeBlase, K. E. Silberstein, T.-T. Truong, H. D. Abruña, W. R. Dichtel, *J. Am. Chem. Soc.* **2013**, *135*, 16821–16824; b) C. R. Mulzer, L. Shen, R. P. Bisbey, J. R. McKone, N. Zhang, H. D. Abruña, W. R. Dichtel, *ACS Cent. Sci.* **2016**, *2*, 667–673; c) V. S. Vyas, V. W.-h. Lau, B. V. Lotsch, *Chem. Mater.* **2016**, *28*, 5191–5204.

[7] a) Q. Fang, S. Gu, J. Zheng, Z. Zhuang, S. Qiu, Y. Yan, *Angew. Chem. Int. Ed.* **2014**, *53*, 2878–2882; *Angew. Chem.* **2014**, *126*, 2922–2926; b) H. Xu, J. Gao, D. Jiang, *Nat. Chem.* **2015**, *7*, 905–912; c) S. Lin, C. S. Diercks, Y.-B. Zhang, N. Kornienko, E. M. Nichols, Y. Zhao, A. R. Paris, D. Kim, P. Yang, O. M. Yaghi, C. J. Chang, *Science* **2015**, *349*, 1208–1213; d) H.-S. Xu, S.-Y. Ding, W.-K. An, H. Wu, W. Wang, *J. Am. Chem. Soc.* **2016**, *138*, 11489–11492.

[8] a) S. Dalapati, S. Jin, J. Gao, Y. Xu, A. Nagai, D. Jiang, *J. Am. Chem. Soc.* **2013**, *135*, 17310–17313; b) S.-Y. Ding, M. Dong, Y.-W. Wang, Y.-T. Chen, H.-Z. Wang, C.-Y. Su, W. Wang, *J. Am. Chem. Soc.* **2016**, *138*, 3031–3037; c) Z. Li, Y. Zhang, H. Xia, Y. Mu, X. Liu, *Chem. Commun.* **2016**, *52*, 6613–6616.

[9] a) X. Feng, L. Chen, Y. Honsho, O. Saengsawang, L. Liu, L. Wang, A. Saeki, S. Irle, S. Seki, Y. Dong, D. Jiang, *Adv. Mater.* **2012**, *24*, 3026–3031; b) M. Dogru, M. Handloser, F. Auras, T. Kunz, D. Medina, A. Hartschuh, P. Knochel, T. Bein, *Angew.*

Chem. Int. Ed. **2013**, *52*, 2920–2924; *Angew. Chem.* **2013**, *125*, 2992–2996.

[10] N. A. A. Zwaneveld, R. Pawlak, M. Abel, D. Catalin, D. Gigmes, D. Bertin, L. Porte, *J. Am. Chem. Soc.* **2008**, *130*, 6678–6679.

[11] S. Wan, J. Guo, J. Kim, H. Ihee, D. Jiang, *Angew. Chem. Int. Ed.* **2008**, *47*, 8826–8830; *Angew. Chem.* **2008**, *120*, 8958–8962.

[12] W. Huang, Y. Jiang, X. Li, X. Li, J. Wang, Q. Wu, X. Liu, *ACS Appl. Mater. Interfaces* **2013**, *5*, 8845–8849.

[13] a) H. M. El-Kaderi, J. R. Hunt, J. L. Mendoza-Cortés, A. P. Côté, R. E. Taylor, M. O'Keeffe, O. M. Yaghi, *Science* **2007**, *316*, 268–272; b) S. B. Kalidindi, C. Wiktor, A. Ramakrishnan, J. Weßing, A. Schneemann, G. Van Tendeloo, R. A. Fischer, *Chem. Commun.* **2013**, *49*, 463–465; c) C. Qian, S.-Q. Xu, G.-F. Jiang, T.-G. Zhan, X. Zhao, *Chem. Eur. J.* **2016**, *22*, 17784–17789.

[14] a) S. Kandambeth, V. Venkatesh, D. B. Shinde, S. Kumari, A. Halder, S. Verma, R. Banerjee, *Nat. Commun.* **2015**, *6*, 6786; b) A. Halder, S. Kandambeth, B. P. Biswal, G. Kaur, N. C. Roy, M. Addicoat, J. K. Salunke, S. Banerjee, K. Vanka, T. Heine, S. Verma, R. Banerjee, *Angew. Chem. Int. Ed.* **2016**, *55*, 7806–7810; *Angew. Chem.* **2016**, *128*, 7937–7941.

[15] P. Pachfule, S. Kandmabeth, A. Mallick, R. Banerjee, *Chem. Commun.* **2015**, *51*, 11717–11720.

[16] a) S. Wan, F. Gándara, A. Asano, H. Furukawa, A. Saeki, S. K. Dey, L. Liao, M. W. Ambrogio, Y. Y. Botros, X. Duan, S. Seki, J. F. Stoddart, O. M. Yaghi, *Chem. Mater.* **2011**, *23*, 4094–4097; b) A. Nagai, X. Chen, X. Feng, X. Ding, Z. Guo, D. Jiang, *Angew. Chem. Int. Ed.* **2013**, *52*, 3770–3774; *Angew. Chem.* **2013**, *125*, 3858–3862.

[17] a) R. B. Zerdan, N. T. Shewmon, Y. Zhu, J. P. Mudrick, K. J. Chesney, J. Xue, R. K. Castellano, *Adv. Funct. Mater.* **2014**, *24*, 5993–6004; b) M. Grzybowski, D. T. Gryko, *Adv. Opt. Mater.* **2015**, *3*, 280–320; c) M. Stolte, S.-L. Suraru, P. Diemer, T. He, C. Burschka, U. Zschieschang, H. Klauk, F. Würthner, *Adv. Funct. Mater.* **2016**, *26*, 7415–7422.

[18] Q. Ge, J. Ran, J. Miao, Z. Yang, T. Xu, *ACS Appl. Mater. Interfaces* **2015**, *7*, 28545–28553.

[19] N. Kameta, H. Minamikawa, M. Masuda, *Soft Matter* **2011**, *7*, 4539–4561.

[20] J.-X. Jiang, F. Su, A. Trewin, C. D. Wood, N. L. Campbell, H. Niu, C. Dickinson, A. Y. Ganin, M. J. Rosseinsky, Y. Z. Khimyak, A. I. Cooper, *Angew. Chem. Int. Ed.* **2007**, *46*, 8574–8578; *Angew. Chem.* **2007**, *119*, 8728–8732.